Characterization of Piezo-driving Actuators to Shake Optical Lattices in High Frequency Regime at least $40kHz$

Supervisor: Joseph H. Thywissen

ZHOU Rongzi

The Chinese University of Hong Kong

A report for Summer Undergraduate Research Exchange program

in the

Department of Physics

of

University of Toronto

September 30, 2019

Abstract

Ultra-cold atoms can be optically trapped in the interference patterns of light, which is also referred to optical lattices. For some quantum properties we need a time dependent Hamiltonian, i.e. shaking the lattice at a certain frequency. However, current devices in our lab couldn't make to high frequencies up to dozens of kilohertz and a high point stability for such frequency regime has always been difficult to achieve. Here by retro-reflecting laser beams with a piezo-driven mirror, we can create such artificial lattices with controllable tuning parameters like effective Hamiltonian, which is crucial for noble quantum simulations. The focus of this project is the characterization of such piezo-driving systems in different configurations. After testing the mechanical resonances and expansion behaviour, we show the $\Phi = 7.0mm$ mirror and Ring type actuator maybe capable for experiments nearby $40kHz$ with high bandwidth and low steering errors.

Chapter 1

Introduction

1.1 Objective and overview

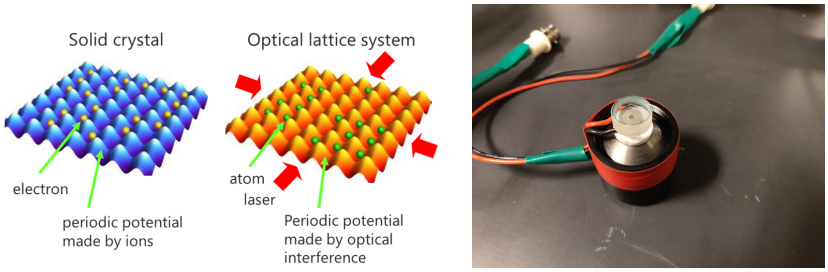

(a) *Crystallized Optical lattice*

(b) *piezo-driving actuator*

Figure 1.1: *Optical lattice and Piezo-driving actuator*

Optical lattices can be produced by retro-reflecting a laser beam from a mirror. Ultracold neutral atoms can be trapped by the spatially periodic potential resulting from the interference patterns. By proper arrangement, trapped atoms resemble a crystal lattice and can be used as quantum simulation, as is shown in Fig 1.1(a)[1]

To modify some quantum properties, we need highly tunable optical lattices, for example, adjusting the lattice depth periodically. This can be done by small displacement of the mirror to create a time-periodic Hamiltonian. So shaking the lattice is the most crucial point for this project, and we achieved it by gluing a mirror to a piezoelectric actuator and driving it with an AC signal. The whole optical lattice shakes due to the oscillation motion of the piezo actuators. Fig 1.1(b) is the photograph of such a device.

1.2 Parameters and Fermi-Hubbard approximation

To know what parameters we need to control when shaking the lattice, we use Fermi-Hubbard model to describe its Hamiltonian,

$$\hat{H} = -t \sum_{<\boldsymbol{j},\boldsymbol{l}>\sigma} (c^{\dagger}_{\boldsymbol{j}\sigma} c_{\boldsymbol{l}\sigma} + c^{\dagger}_{\boldsymbol{l}\sigma} c_{\boldsymbol{j}\sigma}) + U \sum_{\boldsymbol{j}} n_{\boldsymbol{j}\uparrow} n_{\boldsymbol{j}\downarrow} - \mu \sum_{i} (n_{j\uparrow} + n_{j\downarrow}) \tag{1.1}$$

The first term is the kinetic term, describing the destruction of fermion of spin σ on site $\boldsymbol{l}$ and its creation on site $\boldsymbol{j}$, allowing for tunneling only between adjacent lattice sites. The second term is the interaction term, going through all the sites and adding an energy U for doubly occupied site. The last term is the filling term with chemical potential μ, which could also be half-filling when there's only one Fermion per site.

As derived by Sandra Boub, if the actuator is driven by a sinusoidal signal, the mirror shakes with angular frequency $\omega_{lat} = 2\pi f_{lat}$ and real peak to peak amplitude is A_{pp}, then the lattice potential is periodic with $V_{lat}(x - x_0(\tau))$, where $x_0(\tau) = \frac{1}{2} A_{pp} sin(\omega_{lat}\tau)$. This leads to a time-dependent inertial force $F(\tau) = -m\ddot{x_0}(\tau)$. In the lattice frame,

$$\hat{H}(\tau) = \frac{\hat{p^2}}{2m} + V_{lat}(\hat{x}) - F(\tau)\hat{x} \tag{1.2}$$

Going back to the Hubbard model, if we neglect the interaction term, the Hamiltonian turns to

$$\begin{aligned} \hat{H} &= -t \sum_{<\boldsymbol{j},\boldsymbol{l}>\sigma} (c^{\dagger}_{\boldsymbol{j}\sigma} c_{\boldsymbol{l}\sigma} + c^{\dagger}_{\boldsymbol{l}\sigma} c_{\boldsymbol{j}\sigma}) - F(\tau) \sum_{i} ia\hat{n}_i \\ &= -t \sum_{<\boldsymbol{j},\boldsymbol{l}>\sigma} (c^{\dagger}_{\boldsymbol{j}\sigma} c_{\boldsymbol{l}\sigma} + c^{\dagger}_{\boldsymbol{l}\sigma} c_{\boldsymbol{j}\sigma}) - \hbar\omega_{lat} K_0 sin(\omega_{lat}) \sum_{i} ia\hat{n}_i \end{aligned} \tag{1.3}$$

where K_0, the normalized energy difference between adjacent lattice sites due to the inertial force is given by

$$K_0 = \frac{F_0 a}{\hbar\omega_{lat}} = \frac{\pi a m}{\hbar} A_{pp}[\mu m] f_{lat}[kHz] \tag{1.4}$$

F_0 is the amplitude of inertial force and m is the mass of fermions.[2]

Above derivations are quoted from Sandra Boub's thesis. Therefore we know, to create an optical lattice with a desired energy, the most important parameters to control are mirror's full displacement A_{pp} during a whole period and its shaking frequency f_{lat}.

Chapter 2

Equipment and Design

2.1 Piezo-driving system

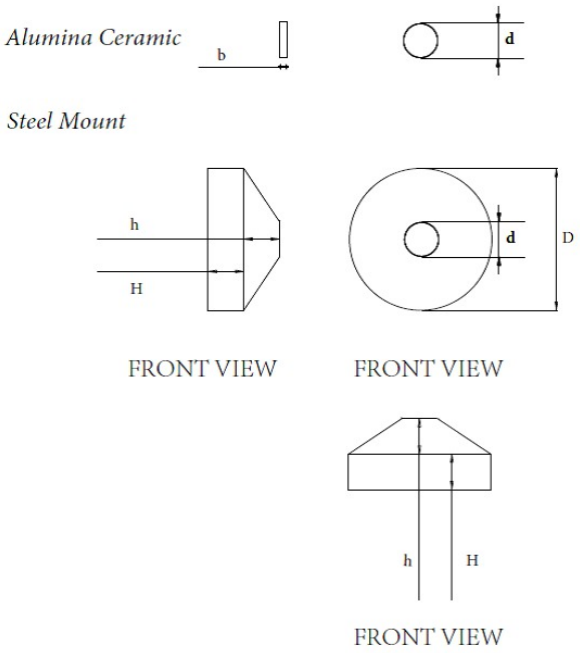

b can be ranging from 2.0 to 5.0mm, d=12.6mm,
H=20.0mm, h=50.0mm, D=25.0mm,

Figure 2.1: *Schematic of Piezo Driving system*

Firstly, we want to go through more in-depth the design of the piezo-driving system, which is composed of four parts. A heavy steel-support compatible with the size of existing mirror mount, acts not only as a support, but as a mechanical insulator [2]

to prevent resonances in the frequency regime we're interested in. A piezoelectric actuator, as we mentioned before, shakes the lattice driven by an AV voltage. Between the piezo and the steel-support is an alumina ceramic, playing the role of an electrical insulator. A mirror is affixed to the actuator it to retro-reflect laser beam. All surface bonds are made with epoxy resin. Schematic for the steel support and ceramic is shown in Fig 2.1

2.1.1 Steel-support and resonance

There are two annoying resonances affecting the behavior dramatically. The first one is drumhead-like vibrations of the mounting face, which can be regarded as imbalanced expansion at different positions near the mounting face. It could cause periodic transversal laser beam deflections as shown in Fig 2.2, which is also referred to "micromotion". The second one is longitudinal compression resonance, which could cause unexpected troublesome phase shift. A research team proposed that, it may be helpful to mitigate these resonance effects by tapering the support structure and filling it with lead [3], whose design is shown in Fig 2.3, but I didn't get enough time to implement and test this idea.

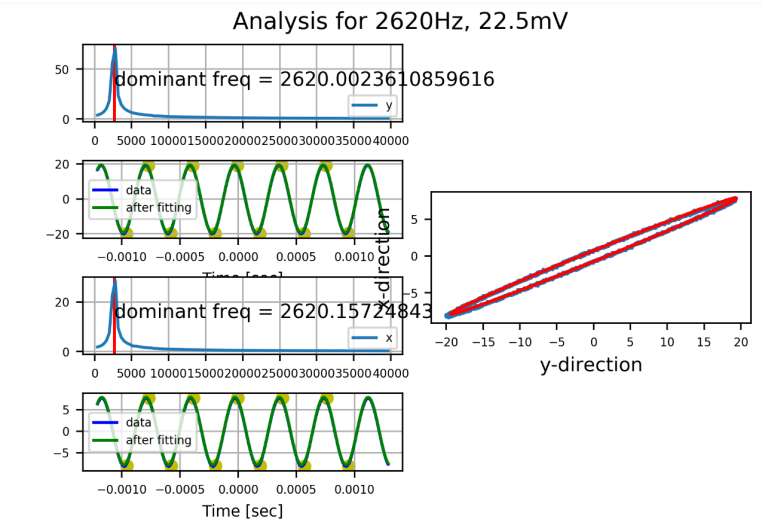

The left side is the real-time coordinates of the laser beam illuminated on a quad photo-diode, and the right side is the trajectory after several periods

Figure 2.2: *A demo of the Micro-motion due to drumhead-like vibrations*

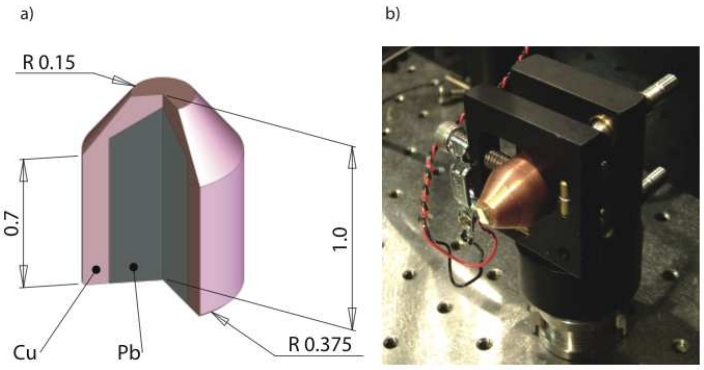

(a)Schematic of the support structure, where all unit are in inches
(b)A photograph of the actuator in a mirror mount

Figure 2.3: *Design of piezo-driving system*

2.1.2 Configurations of Piezoelectric actuator

We bought three types of piezoelectric actuators and their essential properties are tabulated below[4].

	Noliac	**Tripod**	**Ring**
Model	NAC2013	NAC2012(×3)	NAC2121
Shape	square	3×square	ring
Dimensions(mm)	5×5×2	3×3×2	6-2×2
Capacitance (nF)	190	65(each)	105
Voltage range (V)	0∼150	0∼150	0∼200
Max Stroke (μm)	3.3(normal)	3.3(normal)	3.3(normal)
Stiffness (N/μm)	318	115	321

Even though steel mounts could mitigate resonance acting as mechanical insulator, it's still crucial to deal with it from the sources. We expect piezoelectric actuators to be the major source of drumhead-like vibrations, especially the boundary effects at the edges. We expect to mitigate this effect either by choosing a more symmetric geometry configuration or by decreasing the relative size between the actuator and mirror (it will be discussed in details in section 3.4). That's the reason why we expect smaller micro-motion for the Ring and Tripod configurations.

All of these samples have the same maximal stroke of $3.3\mu m$, but their voltage range are different, which means, if we assume the actuator expands linearly as we increase driving voltage, the Noliac and Tripod types can make larger displacement compared to the Ring Type. Normally we won't be able to achieve the maximum stroke, but

using above properties together with the capacitance, we can estimate the maximum possible displacement in real experiments. I will explain it more clearly in the next section.

2.1.3 Kinetic behavior and mass of mirror

We can gain some insights into the kinetic behavior of this Piezo-driving system by modeling it as coupled oscillators. Define x unloaded expansion of the piezo, x_0 true displacement of the mirror, v to be the applied voltage, and k to be the stiffness of piezo. We assume x linearly proportional to v.

$$\begin{aligned} x &= \alpha v \\ L &= x - x_0 \\ F &= kL = k(x - x_0) \end{aligned} \tag{2.1}$$

By Newton's equation, considering damping factor $c = 2\zeta\sqrt{km} = 2m\zeta\sqrt{k/m} = 2m\zeta\omega_n$

$$m\ddot{x_0} + k(x_0 - \alpha v) + c\dot{x_0} = 0 \tag{2.2}$$

Solving this ODE by Fourier Transform, we have

$$\begin{aligned} \alpha_0(\omega) &= \frac{x_n(\omega)}{v(\omega)} = \frac{\alpha\omega_n^2}{\omega_n^2 + 2i\zeta\omega_n\omega - \omega^2} \\ \alpha_0(f) &= \frac{\alpha f_n^2}{f_n^2 + 2i\zeta f_n f - f^2} \end{aligned} \tag{2.3}$$

Hereby α_0 by definition is the mirror's displacement per unit volt. From this equation, we can predict a natural resonance at around $f = \sqrt{\frac{k}{m}}/(2\pi)Hz$.

We expect lighter mirror to be better than massive ones for two reasons: (1)lighter mirror has larger acceleration given the same force, which is crucial for the mirror to attain the required displacement especially driven at high frequency. (2)with lighter mirror we can push the natural resonance to higher frequencies by above equation.

2.2 Piezo controller

We use Piezo controller to drive our piezo-driving actuators, which is literally a series of amplifiers with adjustable DC voltage offset. Normally we can't drive our actuators

with a wave generator directly, because (1)the voltage is not large enough for a proper displacement, and (2)negative voltage may have permanent damages to our piezoelectric actuators, so we need a positive offset. Its performance can be characterized by two properties, the gain for output and the maximum allowed current I_{max}.

I_{max} is critical because piezoelectric actuator, as an capacitor, flows a current limited by

$$I_{rms} = \frac{VppC\pi f}{\sqrt{2}} \tag{2.4}$$

where V_{pp} is the peak to peak voltage applied to piezo actuator.

Take Noliac for example, if we drive it at $40kHz$ with AC voltage $V_{pp} = 25V$ (which normally provide an A_{pp} of 500nm), then the I_{max} should at least be on the order of $(25V) \times (190nF) \times \pi \times (40kHz)/\sqrt{2} \approx 0.4A$. We may estimate the maximum driving frequency by setting $I_{rms} = I_{max}$ and substituting capacitance and voltage range of the actuator into equation 2.4 because capacitance of other parts are negligible. Theoretically, f_{max} for Ring and Tripod type is roughly two times larger than that of the Noliac type.

In our experiment, we used an external, commercial piezo driver PX200 to driven our system, which has a gain of 20V/V for the output voltage and $I_{rms} = 1.5A$. However, we can also drive it with a homemade device by connecting several amplifiers in parallel. For example, Texas Instruments LM7171 can hold a maximum flow of 100mA, then four or five of it in parallel is capable for the case above. The second choice is several hundreds times cheaper than buying a piezo controller, but may induce noises when several amplifier compete with each other. However, we can combine them to drive multiple input systems like the Tripod type. A schematic of such controller is proposed by E. Magnan [5] as Fig 2.4.

This system can provide three different offsets by adjusting corresponding variable resistors. Small resistors (1Ω) are inserted in series to decouple these four parallel amplifiers. We may use other amplifiers for higher current capacitance since our high voltage driver can hold current up to $1.5A$.

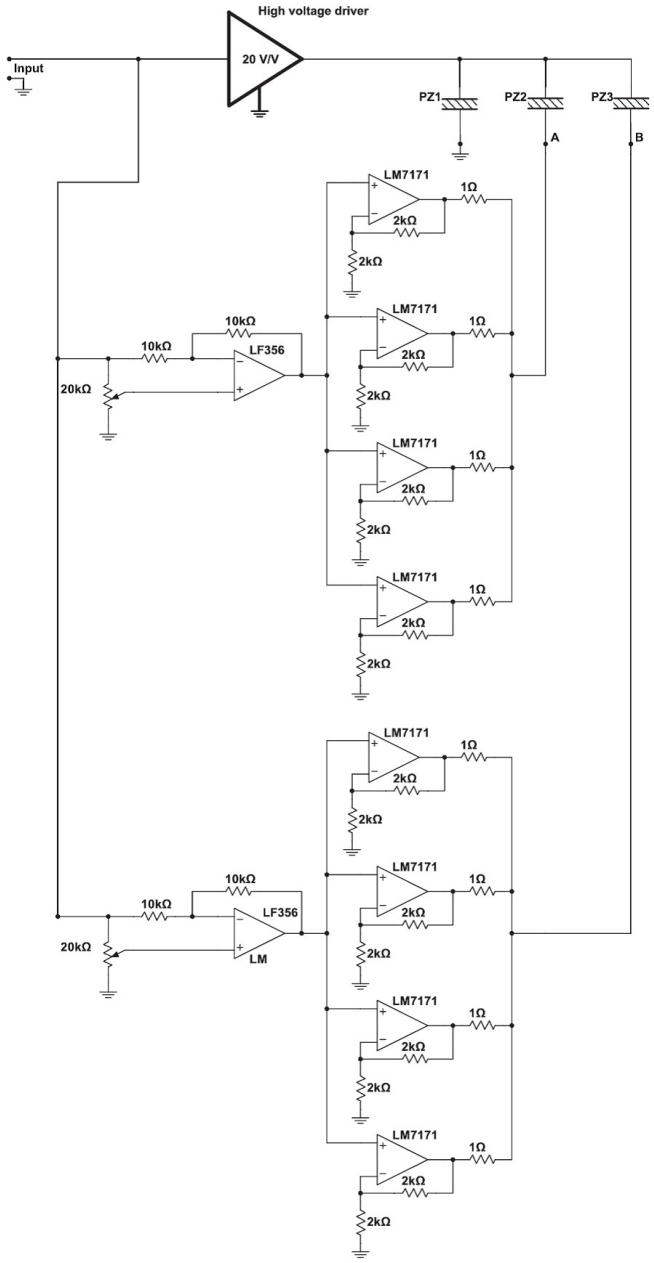

Figure 2.4: *Design of piezo-driving system*

2.3 Michelson Interferometer

To detect tiny expansion of the piezo, we built a Michelson interferometer. For a monochromatic light, it goes through this interferometer and results in two laser beams with $E_1(x,t) = E_{out}e^{i\omega t - kx - 2kd_1}$, $E_2(x,t) = E_{out}e^{i\omega t - kx - 2kd_2}$, where $k = \frac{2\pi}{\lambda}$ and $\omega = ck$.

They interfere with each other and the light intensity measured by photo-diode is

$$I_{out} \propto E_{tot}E_{tot}^{*} = 2E_{out}^{2}(1 + cos2k(d_1 - d_2)) \tag{2.5}$$

$$= 2E_{out}^{2}(1 + cos\frac{4\pi(d_1 - d_2)}{\lambda}) \tag{2.6}$$

In our experiment, $d_1 - d_2$ equaled to ΔL plus a constant. We could drop that constant since it only contributed to an offset, which could be compensated by the piezo controller. Then intensity $I_{out} \propto cos\frac{4\pi\Delta L}{\lambda}$, and from constructive to destructive interference implies a displacement of $\lambda/4$.

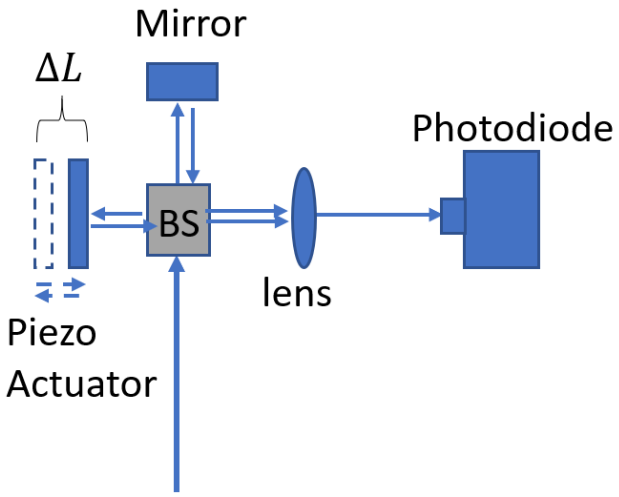

Schematic of Michelson interferometer. The incoming beam goes through a 50/50 cube, then the resulting beams are reflected from a reference mirror and the mirror attached to piezo respectively. ΔL shows the displacement of the mirror due to the piezo's oscillation.

Figure 2.5: *Design of piezo-driving system*

The most difficult part is the alignment. We replaced the photo-diode with a camera and drove the piezo at low frequency (≈1Hz) and low voltage (roughly one fringe of interference pattern). Adjusting the knob while keeping an eye on the camera until a clear light spot flashes in a period of roughly 1s.

Chapter 3

Characterize the piezo-driving system

Discussion in section two gives us insights on several crucial factors to ideal performances (i.e. a flat amplitude and phase response over the entire bandwidth with least unpredicted resonance and steering error). To inspect whether those expectations were correct or not, and also to find the most suitable configuration for our experiment (at least 40kHz with 500nm displacement), it is essential to know how different configurations of piezo-driving system behave at a certain range of shaking frequency and voltage. So in this section we want to characterize four properties: the frequency response, the maximum displacement, the amplitude of the static steering-error and micro-motion. Due to the shortage of time, we only built three piezo actuators as shown in Fig 3.1 below. For simplicity, we call these configurations type I, II, and III respectively.

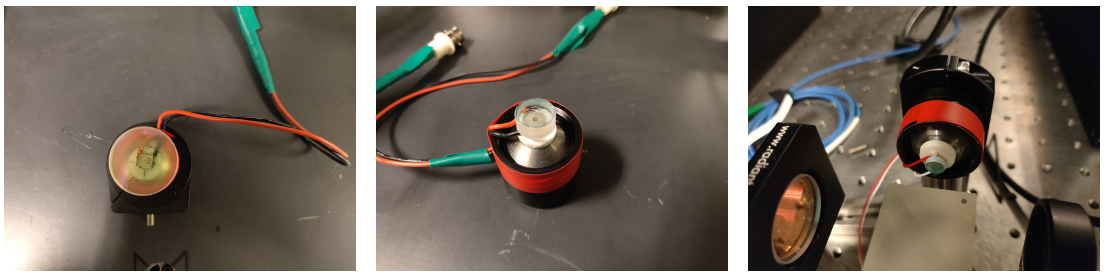

(a) *Noliac* $\Phi = 25mm$, $m = 6.80g$

(b) *Ring* $\Phi = 12.5mm$, $m = 1.68g$

(c) *Square* $\Phi = 7.0mm$, $m = 0.18g$

Figure 3.1: *Three set of actuators we built.*

3.1 Frequency response

Mirror's displacement per unit volt α_0 and the phase shift between mirror's motion and driving signal varies at different shaking frequencies. We refer them to "frequency response".

In equation 2.3, we approximated the possible behavior of α_0 at different frequencies merely based on kinetic factors. If that approximation is reasonable, we may have a rough idea of possible resonances only based on the configuration of piezo and mirror.

To investigate (1)whether our three piezo-driving systems are capable for the experiment within 40kHz, and also to test (2)whether spring model is a reasonable approximation, we need to fit collected α_0 at different f into our model with k, m, and $alpha$ as fitting parameters.

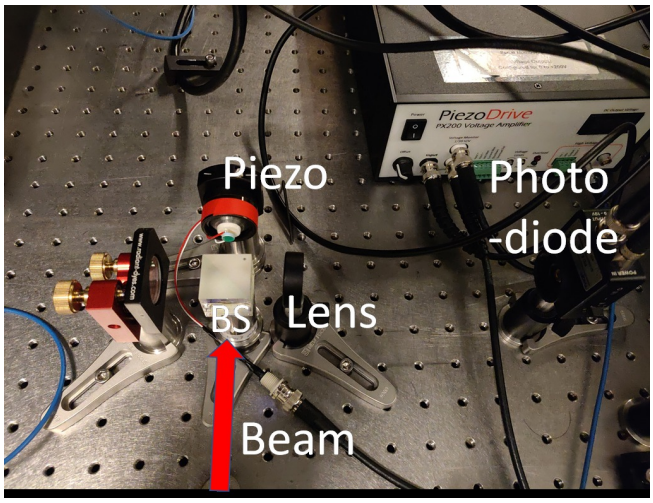

Figure 3.2: *Experimental setup for frequency response and maximum displacement*

The Experimental setup is shown schematically in Fig 2.5, and Fig 3.2 is the photograph. For the whole experiment, we drove the piezo-driving system with a sinusoidal AC signal of a fixed small V_{pp}, satisfying mirror's full displacement $A_{pp} < \lambda/4$. The response signal was controlled at a constant offset by adjusting the piezo controller. The reason why we demanded $A_{pp} < \lambda/4$ is that we wanted a nice sinusoidal response signal easy to calculate its phase and amplitude. Fig 3.3 (a) is an example when $\lambda/4 = 192nm$, $A_{pp} \approx 66nm$ and the mean value was $0.1V$. We fixed the offset because from equation 2.6 we knew the light intensity was affected by the value of offset greatly, as is demostrated in Fig 3.3 (b).

Since interferometer was sensitive to even unwanted small disturbance, we applied a low pass filter to the raw data to filter out high frequency noises and then fitted the

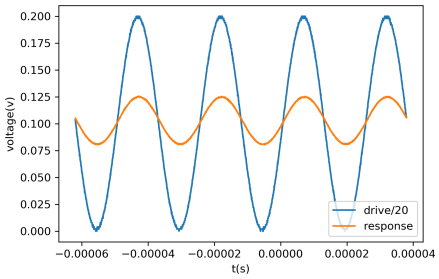

(a) *Example of one pair of the raw data*

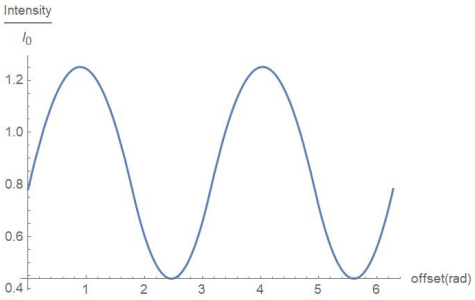

(b) *A demo how offset can affect light intensity measured by the photo-diode*

Figure 3.3: *Raw data and offset.*

response and driving signal with sine functions respectively to obtain their amplitudes (denoted by V_{diode} and V_{drive}) and phases (denoted by Φ_1 and Φ_2). Then α_0 could be calculated by

$$\alpha_0 = \frac{x_0}{V_{drive}} = \frac{\frac{V_{diode}}{V_{\lambda/4}} \times (\lambda/4)}{V_{drive}} \tag{3.1}$$

where $V_{\lambda/4}$ was the voltage difference between constructive and destructive interference. The phase shift was deliberately calculated by $|\Phi_1 - \Phi_2| \bmod \pi/2$ so that we can identify rate of change easily.

After scanning the frequency regime we were interested in, we obtained the results as shown in Fig 3.4. Now we can answer the two questions raised in the beginning of this section.

For question (1), the main criterion is whether we will meet resonances near $40kHz$. Huge peaks of phase shift and α_0 indicate resonances. In Fig 3.4(a) we observed both of these peaks. In Fig 3.4(b), even though no clear peaks occured, the increase of α_0 by roughly 50% implies a peak at higher f not far away. As for Fig 3.4(c), apart from tiny fluctuations, the overal response is flat and stable. Therefore, in comparison, type I and II are not capable for experiments within $40kHz$ due to resonances while type III is capable.

For question (2), the criterion is whether we can fit raw data with our model and predict those fitting parameters. When scanned frequency close to f_n like Fig 3.4(a) and (b), theoretical values of α, f_n and damping factor ξ predicted by our model corresponds pretty well with the fitting results. For Fig 3.4(c), since the scanned frequency was too far from f_n, the frequency response was flat so the relative error became thus not negligible. That may be the reason why our prediction of f_n differed by two times from the fitted value, but other parameters fitted quite well. However, it's still reasonable

to guess a resonance near $200kHz$ and we could do a measurement nearby to test it. Overall, the fitted f_n increases and ξ decreases for smaller mirrors, which is reasonable. However, in my measurement, I also met several resonances far away from f_n like Fig 3.4(d), and our model just failed in these cases. Therefore, we do gain some idea of the response behaviour from this model, and I am sure if we can deal with random errors the fitting result should be much more better even far away from f_n, but we can't rely on it to predict resonance due to other resources just as indicated by Fig 3.4(d).

In summary, a smaller mirror can give us a relatively flat frequency response by pushing resonance to higher values as we predicted, so only type III is capable of the experiments near $40kHz$. Our spring approximation is reasonable but breaks down when other factors like edge effects came into effect. What's more, as a system coupling mechanical and electric factors, it will do great favor and give us more accurate prediction if we count in piezoelectric effect.

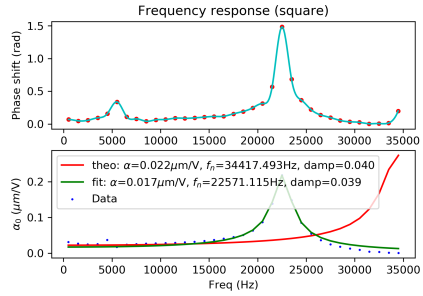

(a) *Square actuator with* $\Phi = 25.0mm$

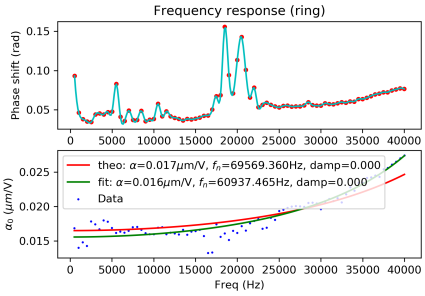

(b) *Ring actuator with* $\Phi = 12.5mm$

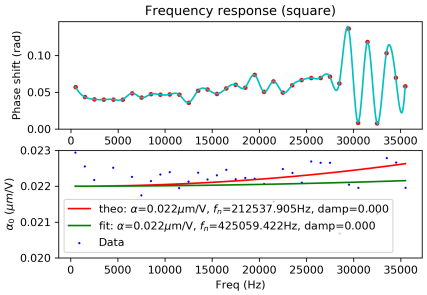

(c) *Square actuator with* $\Phi = 7.0mm$ *at* $f < 40kHz$

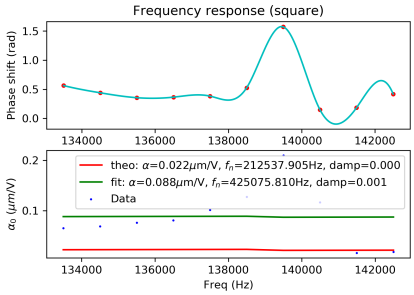

(d) *Square actuator with* $\Phi = 7.0mm$ *at* $f > 130kHz$

Figure 3.4: *Experimental results*

3.2 Maximum displacement

Characterization of the maximum displacement involved the same setup as the last section. For each configuration, we picked five frequencies and for each frequency, we applied the piezo with a AC sinusoidal signal. The peak to peak voltage V_{pp} ranged up to 70V so that we can investigate the maximum displacement. Since V_{pp} was large enough to produce multiple interference patterns, row data collected looked no longer a sine function, but a periodic curve plotted in Fig 3.5 (the blue curve labeled as "response"). We made some amends to Sandra's method and analyzed these data using Python. The rough idea is to firstly apply a low pass filter to both the driving signal and response signal to eliminate random high frequency errors, and then use a sine function to fit the driving signal so as to cut them into a single period of the driving voltage as enclosed by the red rectangle. Then smooth the data by using the mean value (red dot) to represent n data points. Finally, the peak to peak displacement amplitude A_{pp} is given by

$$A_{pp} = \frac{1}{2}\frac{\lambda}{2}\frac{\sum_j \Delta V_j}{2D} \tag{3.2}$$

where ΔV_j is the relative voltage difference between nearby two red dots and D is the voltage difference between the constructive and destructive interference.

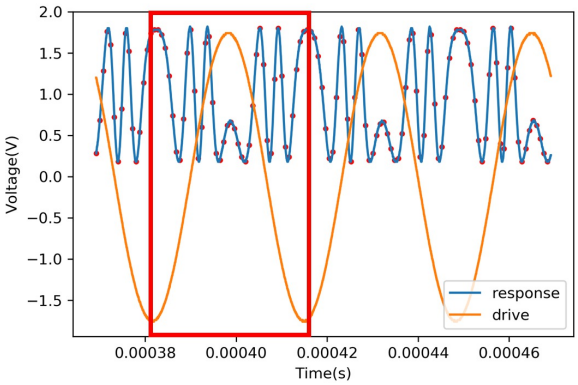

Figure 3.5: *Illustration of raw data and analysing procedure*

Experimental result is shown in Fig 3.6.

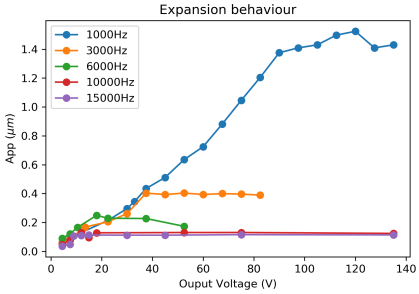

(a) *Saturation when maximum current is achieved*

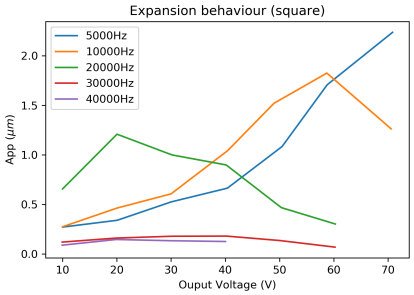

(b) *Square actuator with* $\Phi = 25.0mm$

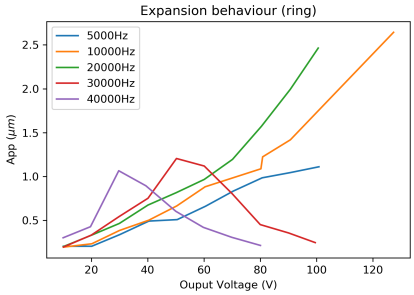

(c) *Ring actuator with* $\Phi = 12.5mm$

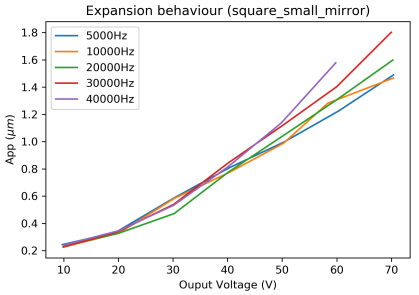

(d) *Square actuator with* $\Phi = 7.0mm$

Figure 3.6: *Experimental results*

Previously we assumed a linear relationship between the mirror's displacement and the driving voltage, but it wasn't always the case. The most common problem we might encounter is the saturation of the piezo controller as we discussed in section 2.2. As shown in Fig 3.6(a), we drove the type I actuator with a piezo controller of $I_{max} = 60mA$, and plateau appeared as we increased the V_{pp}. To inspect whether the plateaus raised because of saturation, for each turning point, we picked its f and V_{pp} and substituted these values together with I_{max} into equation 2.4. We calculate the

capacitance for the whole system to be $\approx 1.91nF$, which was very close to the labeled value $1.9nF$. So our idea is verified.

However, when we changed another piezo controller with $I_{max} = 1.5A$, we still couldn't get a linear relationship for type I and II as shown in Fig 3.6(b) and 3.6(c). The current at the turning point was far below the I_{max}, so this time the nonlinearity shouldn't because of saturation of piezo controller. I didn't have time to figure out why this phenomenon appeared but I guess mechanical factors played the crucial role. Because a nice linearity is observed in Fig 3.6(d) and the only difference between the actuators in Fig 3.6(b) and 3.6(d) was the mass of the mirror. One possible reason is the system with larger mirror should has smaller acceleration. The larger f was, the less distance the mirror traveled before acceleration changed direction. So that might be why A_{pp} declined as f increased.

In summary, the crucial point for a good linearity is a piezo controller with larger I_{max} and a piezo-driving system with smaller mirrors.

3.3 Static steering error

We met this problem in the measurement of the maximum displacement. As the driving voltage increased, we found $V_{\lambda/2}$ shrunk. Then we adjusted the knobs of the reference mirror and $V_{\lambda/2}$ returned to its previous value. Therefore, we guess the static steering error might resulted from the misalignment of Michelson Interferometer because of a constant tilt of the piezoelectric actuator as the voltage increases. I didn't have time to investigate the source of such a tilt but a possible candidate is imbalanced thermal expansion of the piezoelectric actuator. Thus we expected this misalignment to be more severe for higher frequency and higher driving voltage.

To test our idea, we used the experimental setup shown schematically in Fig 3.7 to measure how far the beam moved from its original position as V_{pp} increased. The displacement was calculated by comparing the position of the beam spot measured by a quadruple photodiode before and after adjusting the driving voltage. A series of mirrors were set to amplify the displacement. We picked several frequencies from $5kHz$ to $40kHz$, and for each frequency, we scanned the driving voltage up to $V_{pp} = 60V$. The data we collected was the voltage signal measured by the photo-diode instead of the true position. Therefore, to transfer from voltage signal V to true position, we made a calibration using a kinetic mirror mount with a micrometer and obtained $\theta = nV$, where θ is the tilt angle from the central of the quad photodiode and $n = 234(\mu rad/m)/V$ in our case.

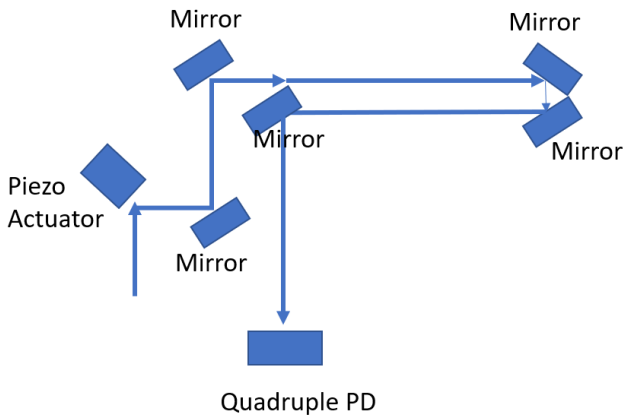

Figure 3.7: *Experimental setup for Static steering error and micromotion*

The crucial point for this section is to adjust the initial position of the laser beam because the photodiode is the most sensitive near the central. We achieved this by making "SUM" channel of the quad photodiode to be as large as possible, while "X" and "Y" channel as close to 0 as possible. We also need to make sure it is not saturated. The experimental result is shown in Fig 3.8.

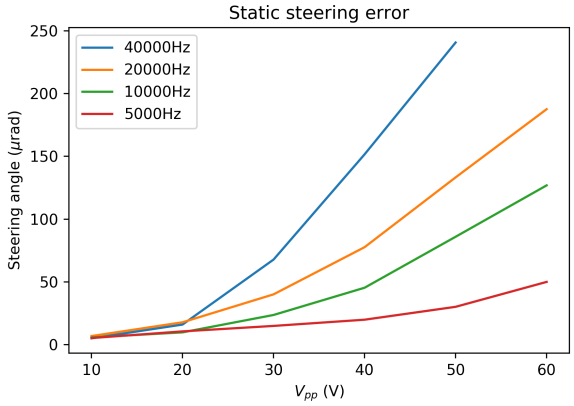

Figure 3.8: *Static steering error with unit $\mu rad/m$*

What we cared about is (1)how does it related to V_{pp} and (2)order of the magnitude. As we predicted before, the steering angle increased for larger frequency and higher voltage amplitude, which might because imbalance of thermal expansion became severe for these cases. The steering angle had an order of dozens μrad for $V_{pp} < 30v$. However, we shouldn't be worried too much about this error since it is relatively a static tilt which can be compensated by making alignment again, but it is really annoying to realign the beams every time you increases the driving voltage. Professor Joseph suggested

that we may use a set of lenses to mitigate this error, but I didn't get enough time to implement this idea.

3.4 Micromotion

Comparing to the static steering error, the micromotion is more troublesome because it is a time-dependent transversal deflection of the laser beam, which is difficult to do a real-time compensation. The optical lattice will simply move in arbitrary directions and even become unable to trap atoms if this error was too large.

Since micromotion is also a piezo driving motion, it's reasonable to expect larger micromotions when we increase V_{pp}. Another possible factor affecting the amplitude of micromotion should be the geometry of our piezo just as we discussed in section 2.1. We expect larger micromotion for Noliac type compared to Ring type due to more sever boundary effect of the square shape compared to the ring shape.

Our aims for this section were (1) to investigate possible factors affecting the amplitude of micromotion (2) to know its order of magnitude. Data analysis method was the same as section 3.1, and the experimental setup was the same as that for section 3.3. We drove the piezo with a sinusoidal signal scanning the frequency within $3kHz$, and for each frequency, the V_{pp} varied from 0 to 30V. Theoretically, we should go to higher frequency and voltage regime, but when I was doing this part, the new piezo actuator still haven't arrived and I didn't have enough time to redo it afterwards.

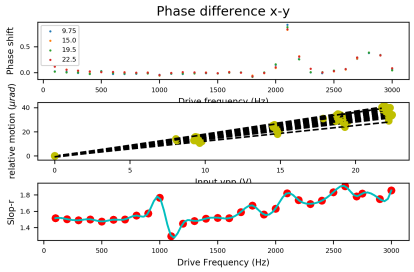

(a) *Micromotion for Noliac with* $\Phi = 25mm$

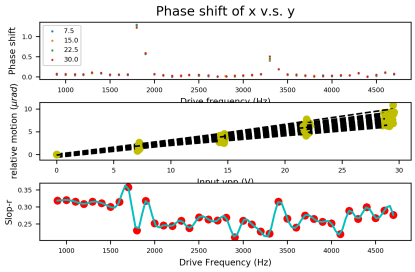

(b) *Micromotion for ring actuator with* $\Phi = 12.5mm$

Figure 3.9: *Micromotion with unit* $\mu rad/m$

For the first aim, from the second raw in Fig 3.9, we can see perfect linearities between the relative motion and V_{pp}, hence our expectation that higher voltage can bring larger micromotion is correct. What's more, we also plotted the slope for each frequency in the

last raw, which implies the amplitude of micromotion per unit volt. Comparing these two types of piezo actuators, we find the slop for type II is roughly four time smaller than that for type I. Therefore, geometry has something to do with micromotion as we predicted. We didn't try the Tripod type but I expect even smaller micromotion if we can drive its three components with different DC offsets. For our second aim, at least for V_{pp} smaller than 30V, which is enough for a lot experiments, the relative motion is less than $10\mu rad/m$ for the Ring type. It is possible to mitigate this motion by adding a lens or a feedback loop, but I didn't have time to implement these ideas.

Chapter 4

Conclusion and outlook

It's reasonable to model the piezo system as coupled spring oscillators and the natural resonant frequencies can be pushed to higher values by adapting mirrors with smaller mass or increasing the stiffness k. The bonus for smaller mirror is the larger maximum displacement for high frequency regime because of possibly some mechanical reasons. The static steering error has larger amplitude than micromotion, but it is static so we can deal with it by realigning laser beams every time we change the V_{pp} dramatically. Micromotion is troublesome because it is a periodic motion and the amplitude increases linearly with V_{pp}. However, we don't need to worry a lot about it since it's quite small in our interested voltage regime and will be even smaller if the piezo's geometry configuration is symmetric. It's possible to mitigate these errors by adding a series of lenses.

After our comparison, type III is already very close to be put into operation. For the next stage, we can (1) rebuild the piezo-driving system with the support in Fig 2.3 to mitigate resonances; (2) test the Tripod type and drive it with the piezo driver shown in Fig 2.4 using different DC offsets for possibly higher maximum frequency and smaller steering errors; (4) test whether a feedback loop or a series of lens can reduce these errors; (5) test our spring model by doing experiments in section 3.1 with higher frequencies near natural resonances; (6) refine our model by counting in other possible factors like piezoelectric effect and boundary effect, and try to figure out the sources of harmonics other than f_n; (7) test the system in real experiment.

Chapter 5

Acknowledgements

I would like to appreciate Professor Joseph H. Thywissen and University of Toronto for the opportunity of joining in lattice group this summer for my first experimental research project. I am also grateful to Professor Wang Dajun for his time and support in arranging my trip. Special thanks to Vijin and Rhys for their intuitive introductions to the background knowledge and inspirations to me in each step during this project. I'd also like to express sincere thanks to the whole team for letting me feel at home even in a foreign country.

Chapter 6

Reference

1 Kozuma laboratory, Department of Physics, Tokyo Institute of Technology`http://www.kozuma-eng.sci.titech.ac.jp/research_category/entry17.html` (2019).

2 S. Buob, Characterization Of Piezoelectric Actuators To Shake An Optical Lattice In A Cold Atom Experiment (Swiss Federal Institute of Technology in Zurich, Switzerland, 2018).

3 T. Briles, D. Yost, A. Cingz, J. Ye and T. Schibli, Optics Express 18, (2010).

4 Noliac Partner, Noliac - Your Piezo Partner `http://www.noliac.com/products/actuators/`(2019).

5 E. Magnan, J. Maslek, C. Bracamontes, A. Restelli, T. Boulier and J. Porto, Review Of Scientific Instruments 89, (2018).